

# High-resolution petrographic evidence confirming detrital and biogenic magnetites as remanence carriers in Zongpu carbonates, South Tibet

1 Qian Zhao<sup>1</sup>, Baochun Huang<sup>1\*</sup>, Zhiyu Yi<sup>2</sup>, Pengfei Xue<sup>1</sup>

2 <sup>1</sup> Key Laboratory of Orogenic Belt and Crustal Evolution, Ministry of Education, School of Earth  
3 and Space Sciences, Peking University, Beijing, China

4 <sup>2</sup> Planetary Environmental and Astrobiological Research Laboratory (PEARL), School of  
5 Atmospheric Sciences, Sun Yat-sen University, Zhuhai, China

6 \* Correspondence:

7 Baochun Huang

8 bchuang@pku.edu.cn

9 **Keywords:** Magnetic extraction, Carbonates, Paleomagnetism, Tethyan Himalaya, Paleocene

## 10 Abstract

11 Paleocene carbonates from the Gamba area of South Tibet provide the largest paleomagnetic  
12 dataset for constraining the paleogeography of the India-Asia collision in the early stage. The  
13 characteristic remanences (ChRMs) obtained from this unit were, however, argued for a chemical  
14 remagnetization via orogenic fluids. This study carries out a high-resolution petrographic study on  
15 the Paleocene carbonates from Gamba aiming to test the nature of the ChRMs. Electron microscopic  
16 observation on magnetic extracts identified a large amount of detrital magnetite that are multi- to  
17 single domain in sizes and biogenic magnetite in nanoscale. Minor framboidal iron oxides were also  
18 identified, which were previously interpreted as authigenic magnetite that substitutes pyrite.  
19 However, our scanning and transmission electron microscopic (SEM/TEM) observations, along with  
20 optical microscope and Raman spectrum investigations further suggest that these magnetic minerals  
21 are pigment hematite and goethite that are incapable of carrying a stable remanence. We therefore  
22 argue that the ChRMs of the limestones from the Zongpu Formation in the Gamba area are carried by  
23 detrital and biogenic magnetites rather than authigenic magnetite. The paleomagnetic data from the  
24 Gamba area are interpreted as primary origin and can thus be used for tectonic reconstructions. We  
25 emphasize that magnetic extraction, integrated with advanced mineralogic studies (e.g., electron  
26 backscatter diffraction and electron diffraction) are effective approaches for investigating the origin  
27 of magnetic carriers in carbonate rocks.

## 28 1 Introduction

29 Consecutive indentation of India into continental Asia resulted in a rapid uplift of the Tibetan  
30 Plateau that has profoundly changed the climatic pattern and topography of Asia since the Cenozoic  
31 era (Yin and Harrison, 2000; Jagoutz et al., 2016). The timing and position of the initial collision  
32 between India and Asia remain highly debated (e.g., Ding et al., 2005; Leech et al., 2005; Aitchison  
33 et al., 2007; Ali and Aitchison, 2008; Najman et al., 2010; Yi et al., 2011; van Hinsbergen et al.,  
34 2012; Hu et al., 2016; An et al., 2021). On the paleolatitudinal comparison based on reliable

35 paleomagnetic poles, paleomagnetism provides a direct constrain on timing and locus for the initial  
36 collision between India and Asia (e.g., Dupont-Nivet et al., 2010; Najman et al., 2010; Yi et al.,  
37 2011, 2021)

38 The Indian plate was subjected to rapid northward motion toward Asia during the Cretaceous  
39 and Paleocene (Patriat and Achache, 1984; Yin and Harrison, 2000; van Hinsbergen et al., 2011).  
40 The kinematics of the northern margin of India can be constrained by the Cretaceous and Paleogene  
41 paleomagnetic data obtained from the Tethyan Himalaya (Besse et al., 1984; Patzelt et al., 1996;  
42 Tong et al., 2008; Yi et al., 2011; Yang et al., 2015, 2019; Ma et al., 2016; Meng et al., 2019, 2020;  
43 Y. Zhang et al., 2019; Yuan et al., 2020). For the lack of contemporary volcanic rocks, the Late  
44 Cretaceous to Paleocene sedimentary rocks from the Tethyan Himalaya are especially crucial for  
45 reconstructing the overall process of the India-Asia collision. Several paleomagnetic poles were  
46 reported from the marine sediments of the Tethyan Himalaya with the Late Cretaceous to Paleocene  
47 in ages (Besse et al., 1984; Patzelt et al., 1996; Tong et al., 2008; Yi et al., 2011; Ma et al., 2016;  
48 Yang et al., 2019; Meng et al., 2020; Yuan et al., 2020). In the light of these poles, a variety of  
49 paleogeographic reconstructions were established with small (Besse et al., 1984; Tong et al., 2008),  
50 moderate (Yi et al., 2011), and enlarged (Meng et al., 2020) Greater India or hypothesized oceanic  
51 basins, namely, “Greater India Basin” (van Hinsbergen et al., 2012) or “North India Sea” (Yuan et  
52 al., 2020).

53 A continuously outcropped marine sedimentary sequence is well-preserved in the Gamba area.  
54 Among these units, the Zongshan (71-65 Ma) and Zongpu (62-56 Ma) formations provide a unique  
55 opportunity for constraining the locus of the Tethyan Himalaya covering a critical stage of the India-  
56 Asia collision. Detailed lithological and biostratigraphic (Willems and Zhang, 1993; Wan et al.,  
57 2002a,b), sedimentological (Li et al., 2015), and geochemical (Wang et al., 2008; Q. Zhang et al.,  
58 2019) investigations provide a solid foundation for paleomagnetic studies.

59 Characteristic remanent magnetizations (ChRMs) reported from the Zongshan and Zongpu  
60 formations in the Gamba area passed positive fold and reversal tests, along with internally consistent  
61 magnetostratigraphy and biostratigraphic ages (71-56 Ma), permitting the original authors interpreted  
62 them as primary (Patzelt et al., 1996; Yi et al., 2011). However, on the detailed rock magnetic and  
63 petrographic studies, along with a reanalysis of the fold test performed on the Zongpu Formation,  
64 Huang et al., (2017a,b) argued for a widespread remagnetization via orogenic fluids in the Gamba  
65 area, and thus the paleomagnetic poles obtained from Zongpu Formation limestones can no longer be  
66 used to constrain the geometry of the India-Asia collision. As a response, Yi et al. (2017) addressed  
67 the reliability of their fold tests performed on the Zongpu and Zongshan formations and argued for an  
68 acquisition of the ChRMs in the early diagenetic stage.

69 On the basis of rock magnetism and SEM observations incorporating EDS analysis, Huang et al.,  
70 (2017a,b, 2019) argued for the presence of abundant authigenic magnetites in carbonates preserved  
71 within the Tethyan domain of Tibet. These authigenic magnetites were suggested to result from a  
72 partial or complete replacement of pyrite crystals/framboids by secondary magnetites that were  
73 responsible for a widespread chemical remagnetization in the Gamba and Tring area, Tethyan  
74 Himalaya (Huang et al., 2017a,b). However, authigenic magnetic minerals are common for marine  
75 sediments due to the diagenesis during the burial process that may alter the combination of magnetic  
76 components (Roberts, 2015 and references therein) and complicate the discrimination of rock  
77 magnetic parameters. The authigenic magnetic spherules cannot be directly related to a chemical  
78 remagnetization (Saffer and McCabe, 1992; Suk et al., 1992), although the ability of carrying stable  
79 remanence of these magnetic spherules remains elusive (Xu et al., 1994; Suk and Halgedahl, 1996).

80 Moreover, as EDS analyses cannot distinguish magnetic particles among magnetite, hematite, and  
81 goethite due to the imprecise measurement of Fe/O ratios (Sun and Jackson, 1994; Xu et al., 1998;  
82 Weil and Van der Voo, 2002; Franke et al., 2007), the arguments by Huang et al., (2017a,b, 2019)  
83 needs to be further studied.

84 In an effort to clarify the type and origin of the magnetic carriers in the Zongpu carbonates, we  
85 carry out a combined study integrating optical microscopy, SEM/TEM observations, and Raman  
86 spectroscopy measurements on thin sections and magnetic extracts of pilot samples from the Zongpu  
87 Formation in the Gamab area, Tethyan Himalaya. By this way, we further evaluated the nature of  
88 ChRMs reported from the Zongpu Formation by previous studies.

## 89 **2 Sampling sites and experimental methods**

90 Figure 1 illustrates the structure of the Indus-Yarlung Zangbo suture zone, in which  
91 paleomagnetic sampling localities and lithostratigraphic units are indicated. Detailed geological  
92 background is available in many previous studies (e.g., Wan et al., 2002a,b; Yi et al., 2011; Li et al.,  
93 2015; Huang et al., 2017a). The Paleocene carbonate rocks of the Zongpu Formation were deposited  
94 in a shallow-marine carbonate ramp on the northern Indian passive margin (Li et al., 2015). The  
95 Zongpu Formation is divided into four members by lithology; massive limestone (Member I), marls  
96 (Member II), nodular limestones (Member III), and well-bedded limestones (Member IV) (Willems  
97 and Zhang, 1993). Polished thin sections were processed on samples collected by Yi et al. (2011). In  
98 addition, block limestone samples of ~1 kilogram in weight was collected from the top of the Zongpu  
99 Formation for a magnetic extraction and SEM/TEM observations (GPS: 28°16'45.28"N,  
100 88°32'46.97" E, Section A of Yi et al. (2011), Figure 1C).

101 Raman spectra measurements were conducted using a Raman spectrometer (LabRAM HR  
102 Evolution) equipped with a laser (excitation wavelength of 532nm) in the School of Earth and Space  
103 Sciences (SESS), Peking University. Laser power was reduced by a filter to about 1 mW to avoid the  
104 transformation of magnetite, goethite, and pyrite (Hanesch, 2009). Data were obtained with a spectral  
105 resolution of  $1\text{cm}^{-1}$  across the  $100\text{-}1500\text{ cm}^{-1}$  wavenumber offset range. The experiment was carried  
106 out under an objective lens with 100 times magnification. Because of the low laser powers, more than  
107 ninety seconds integration time for individual measurements and 10 accumulations were set to  
108 improve the signal-to-noise ratio. In this study, Raman spectra were provided without smoothing or  
109 fitting to present the original results during the measurements.

110 To further examine the magnetic properties, the carbonate rock samples were first disaggregated  
111 and then put in buffered acetic acid dissolves ( $\text{pH} = 4$ ) for several days. Magnetic extraction is  
112 performed using a self-designed magnetic probe extraction apparatus (Figure S1A). the slurry flowed  
113 through a tube with dispersed fine magnetic fractions and pumped continuously around the extraction  
114 equipment. Improved extraction-related procedures, following Hounslow et al. (1999), were used to  
115 avoid dissolution effects of ultrafine magnetic particles in samples (Sun and Jackson, 1994).

116 Magnetic extracts of pilot samples were prepared for SEM observation as thin sections using  
117 resin as an adhesive (Figure S1B). An alternative and highly recommended procedure to prepare  
118 SEM samples was to drop the solutions with magnetic extracts on a monocrystalline silicon wafer  
119 (Figure S1C). To prepare TEM specimens, distilled water with magnetic extracts was moved to a  
120 small container. A rare-earth magnet hovered ~1 cm above the TEM grid which was floated on the  
121 surface of the solutions, to attract magnetic extracts for ~5 min (Figure S1D). EDS, electron  
122 backscatter diffraction (EBSD), and photographs were performed with SEM/ESEM system at SESS

123 and Electron Microscopy Laboratory (EML) in the School of Physics, Peking University. The TEM  
124 was performed using a JEOL 2100 TEM (200kV) at the Institute of Geology and Geophysics,  
125 Chinese Academy of Sciences (IGGCAS).

### 126 3 Results

#### 127 3.1 Optical petrography and Raman spectroscopy analysis

128 An analysis of the iron oxide-sulfide assemblages in the thin sections and magnetic extracts  
129 under reflected white light shows that pyrite-substituted iron oxides were the most abundant  
130 magnetic phase of the Zongpu Formation (Figures 2A-2D, 2I-2L, and S2). On the blood-red internal  
131 color under plane-polarized light (Figures 2E-2H, 2M-2P), we interpret the iron oxides with poor  
132 crystallinity as fine-grained pigment hematite. Goethite phases, displaying intense brownish yellow-  
133 orange internal reflections, are identified around hematite pseudoframboids (Figures 2D, 2J-2L). The  
134 iron sulfides, inferred as pyrite due to the bright-brassy colored reflections with a speckly  
135 appearance, yielded two morphologic groups: (1) framboid spherules (Figures 2A, 2B, and 2I) and  
136 (2) large euhedral grains (Figures 2C and 2D). The abundant occurrence of the pigment hematite and  
137 goethite along calcite boundaries and/or intergranular dissolved voids are noticeable. Contrastively,  
138 the exclusive presence of pyrite (framboids and euhedral grains) is well-preserved in calcite crystals  
139 as inclusions. Magnetite was not identified by optical microscope observation probably due to the  
140 low concentration, although it was supposed to be the main magnetic carrier in the limestones of the  
141 Zongpu Formation (Yi et al., 2011; Huang et al., 2017a).

142 Furthermore, the Raman spectrum investigations indicate the presence of hematite, goethite, and  
143 pyrite (Figure 3). These results are consistent with our observations under the optical microscope. As  
144 compared with the corresponding spectra of minerals shown in Hanesch (2009) and the RRUFF  
145 database (<https://rruff.info>), the offset peaks might well be caused by different crystallinities of the  
146 natural minerals.

#### 147 3.2 SEM observations of magnetic extracts

148 Abundant pure iron oxides were observed from magnetic extracts by SEM observation. These  
149 submicron iron oxide grains are presented in various morphology, consisting of broken-octahedral,  
150 subangular, irregular, and well-rounded crystals (Figures 4A-4J), suggestive of a detrital origin. The  
151 acquired Electron Back-scattering Patterns (EBSPs) for these grains show a spinel pattern (Figures  
152 4M-4P) that confirm a detrital origin for magnetites, although there may be hematite in some cases.  
153 Interestingly, we also found several euhedral magnetic crystals with clear particle boundaries, about  
154 50-100 nm in size (Figures 4K and 4L). Accordingly, we suggest that these submicron and nanoscale  
155 magnetite particles fit the size range of SD and PSD (Dunlop and Özdemir, 1997) and are the  
156 possible remanence carrier in the limestones of the Zongpu Formation in the Gamba area.

157 Despite the frequent occurrence of detrital magnetite, iron oxide spherules were also founded in  
158 the magnetic extracts (Figure 4A). EDS line scanning and mapping show that the iron oxide  
159 assemblage contains S in addition to Fe and O in a form of pseudoframboid (Figure 5). Given that  
160 cosmic spherules usually contain a low content of Ni (Brownlow et al., 1966) which was not detected  
161 by the EDS analysis, we exclude the possibility of cosmogenesis. Along with our observations in thin  
162 sections, we argue that these pseudoframboids are iron (hydr)oxides (hematite and/or goethite) that  
163 are replaced by framboidal pyrite (Suk et al., 1990) or perhaps framboidal greigite (Roberts et al.,  
164 2011).

### 165 3.3 TEM observations of magnetic extracts

166 The TEM observations reveal that magnetic grains with variable grain sizes are commonly  
167 presented in magnetic extracts from the Zongpu Formation (Figures 6A-6D). Further high-resolution  
168 TEM (HRTEM) indicates that the observed *d*-spacing values (Figure 6F), as well as diffraction  
169 patterns (Figure 6G) for the magnetic particles, match well with the crystal structure of  
170 titanomagnetite. All analyzed magnetic minerals, including submicron and nanosized particles, have  
171 clear lattice fringes (Figures 6E and 6F) and sharp diffraction patterns (Figures 6G-6I) which indicate  
172 good crystallinity.

173 Nanosized and euhedral magnetic crystals were also observed under TEM imaging for the  
174 studied samples (Figures 6C, 6I, and 6L). The grain size of magnetite and titanomagnetite ranges  
175 from tens of nm to several  $\mu\text{m}$ , which is consistent with the SD to MD size of magnetite (Dunlop and  
176 Özdemir, 1997). Non-spheroidal iron oxides are observed in TEM. Together with the EDS spectra  
177 (Figures 6J-6L) and mineral morphologies, we believe that the remanence magnetic carrier should be  
178 detrital magnetite and/or euhedral magnetic particles from the Zongpu Formation in the Gamba area.

## 179 4 Discussion

### 180 4.1 Origin of the euhedral magnetite in nanoscale

181 SD euhedral magnetites were observed in the magnetic extracts (Figures 4K, 4L, and 6C). There  
182 are two possible origins for such magnetic particles in sediments: (1) the magnetic inclusion as  
183 erosional detritus from igneous and metamorphic rocks (e.g., Chang et al., 2016) transported by  
184 rivers and ocean currents; (2) biogenic magnetite (Kopp and Kirschvink, 2008). Both types of  
185 magnetic particles are able to carry stable paleomagnetic signals over billions of years (Kirschvink  
186 and Lowenstam, 1979; Tarduno et al., 2006; Tarduno et al., 2010). Usually, most of the magnetic  
187 nanoparticle inclusions hosted within silicate crystals show high content of Si and low content of Ti  
188 that can be identified by EDS analyses (Chang et al., 2016). In this study, however, only very low  
189 content of Si and no Ti were detected from the euhedral magnetic crystals (Figure 6L). Furthermore,  
190 silicate minerals (e.g., plagioclase and clinopyroxene) were not observed in thin sections (Figures 2  
191 and S4), probably due to the low clastic influx and high carbonate saturation during deposition of the  
192 Zongpu Formation (Li et al., 2015). In this case, the origin of euhedral magnetite in nanoscale from  
193 silicate-hosted magnetic mineral inclusions is highly unlikely. We suggest the nanosized and  
194 euhedral magnetic particles are biogenic magnetite that is capable of carrying stable remanences in  
195 limestones (Chang et al., 1987).

### 196 4.2 The possible origin of iron oxide spherules

197 In addition to the detrital and biogenic magnetites observed in magnetic extracts, iron oxide  
198 spherules were also identified from the Zongpu Formation in the Gamba area (Figures 4, 5, and S2).  
199 Several previous studies attribute the remagnetization of carbonates to the replacement of framboidal  
200 pyrite by oxidation that is related to orogenic fluids (see review by McCabe and Elmore, 1989).  
201 However, the photomicrographs of limestone samples in Huang et al. (2017a) present well-preserved  
202 fossils (benthic foraminifer, echinoderm, ostracod, and green algae) with particles/matrix support and  
203 show no sign of orogenic-type fluids (Figure S4, Li and Hu, 2020). Besides, the variations of carbon  
204 and oxygen isotope of bulk carbonate cover the key interval of the Paleocene-Eocene thermal  
205 maximum (PETM) (Q. Zhang et al., 2019). The strontium isotopic ratios ( $^{87}\text{Sr}/^{86}\text{Sr}$ ) of calcite are  
206 comparable with the global oceanic strontium isotope record (Wang et al., 2008) which indicates that

207 the carbonates in the Gamba area have not been altered by orogenic fluids. The origin of iron oxide  
208 spherules should thus be explained in other mechanisms.

209 Suk et al. (1992) proposed different magnetic mineralogy for the primary and remagnetized  
210 carbonates. The iron sulfides (e.g., pyrite framboids) were moderately or completely oxidized to  
211 hematite in the former while a replacement of magnetite occurs in remagnetized carbonates.  
212 Moreover, oxidation of pyrite under modern atmosphere and groundwater conditions produces  
213 goethite and/or hematite (Todd et al., 2003; Sgavetti et al., 2009; Verron et al., 2019). Recently, a  
214 deep abiotic reaction mechanism of pyrite weathering in rocks was proposed which demonstrated that  
215 fracturing and erosion, in addition to atmospheric oxygen, control the reactivity of iron sulfide  
216 oxidation (Gu et al., 2020). Therefore, we suggest the large amounts of iron (hydr)oxides (e.g.,  
217 goethite and hematite) observed in carbonates from the Zongpu Formation in the Gamba area were  
218 more likely oxidized from pyrite under aqueous solutions in contact with the atmosphere.

### 219 4.3 Primary versus secondary origin of the ChRMs

220 The new-formed Superparamagnetic (SP) to stable single domain (SSD) grain-sized magnetite is  
221 a general indicator for chemical remagnetization in carbonates which could well explain the  
222 remagnetization that occurred in the Paleozoic carbonates of North America (Channell and McCabe,  
223 1994; Suk and Halgedahl, 1996; Xu et al., 1998; Elmore et al., 2006). A mix of SP and SD particles  
224 yields wasp-waisted hysteresis loops and distribution of Day plot along the SP-SD mixing line  
225 (Jackson and Swanson-Hysell, 2012). Nevertheless, magnetic minerals in different assemblage and  
226 shape anisotropy can also present contrasting coercivity distributions, resulting in wasp-waisted  
227 hysteresis loops (Jackson, 1990; Roberts et al., 1995; Newell and Merrill, 2000; Zwing et al., 2005).  
228 It is generally difficult to interpret the magnetic grain size and mineralogy by wasp-waisted  
229 hysteresis loops or Day-plot only (Tauxe et al., 1996; Roberts et al., 2018). It also should be cautious  
230 when using a Day diagram to diagnose remagnetization as occasionally ‘false positives’ and ‘false  
231 negatives’ results may present (Jackson and Swanson-Hysell, 2012; Roberts et al., 2018). Moreover,  
232 the validity of application of Day-plot in shallow-water carbonates, which are isolated from aqueous  
233 detrital input, remains unverified (Jackson and Swanson-Hysell, 2012). On the other hand, our  
234 SEM/TEM observations indicate the content of abundant detrital and biogenic magnetites in the  
235 investigated carbonates (Figures 4 and 6). The optical petrography and Raman spectra analyses  
236 present robust evidence that iron (hydr)oxides, i.e., goethite and hematite (Figures 2, 3, and S2),  
237 rather than magnetite, as substitutes of pyrite framboids. The imaginable detrital/biogenic magnetite,  
238 along with goethite and hematite, would yield wasp-waisted hysteresis loops and distribution of Day  
239 plot along the SP-SD mixing line which leads to an incorrect interpretation of remagnetization from  
240 Day plot locations (Huang et al., 2017a,b, 2019).

241 The argument of previous paleomagnetic investigation for a chemical remagnetization of the  
242 carbonate rocks in the Gamba area was mainly based on SEM and EDS interpretation (Huang et al.,  
243 2017a). Whereafter, the same authors performed analogous analytical processes on the Upper  
244 Cretaceous to Paleocene carbonates from the Tingri area in the Tethyan Himalaya and the Upper  
245 Triassic limestones in the eastern Qiangtang block, argued for a widespread remagnetization in the  
246 Tibetan Tethyan domain (Huang et al., 2017b, 2019). However, the critical “authigenic magnetite”,  
247 along with the “orogenic fluids” are only speculated by the authors, regardless that conventional EDS  
248 techniques only have a semi-quantitative character which cannot directly distinguish the exact iron  
249 oxides. On the contrary, the geochemical evidence from the Zongpu Formation precludes the  
250 existence of widespread orogenic fluids as discussed above. Consequently, the remagnetization  
251 mechanism of chemical alteration suggested by Huang et al. (2017a) is problematic.

252 The presence of abundant detrital and biogenic magnetites in the Zongpu limestones precludes  
253 widespread chemical remagnetization in the Gamba area. On the other hand, the occurrence of anatase  
254 in the underlying Jidula Formation suggests that the overlying Zongpu limestones were never heated  
255 over 260°C (Patzelt et al., 1996) and hence exclude a thermal remagnetization in the Gamba area.  
256 Moreover, the ChRMs from Gamba carbonates yielded positive fold and reversal tests (Patzelt et al.,  
257 1996; Yi et al., 2011, 2017), and the paleomagnetic pole from the Zongpu Formation hence meets all  
258 the criteria for a paleomagnetic study ( $R = 7$ ) (Meert et al., 2020). We therefore concluded that  
259 detrital and biogenic magnetites are the main magnetic carriers of primary remanence and the  
260 paleomagnetic results reported by Yi et al. (2011) from the Gamba area can still be used for  
261 paleogeographic reconstruction.

## 262 **5 Conclusion and perspective**

263 The high-resolution petrographic study was carried out on Paleocene carbonates (the Zongpu  
264 Formation) from Gamba, South Tibet. Electron microscopic observation of magnetic extracts  
265 identified abundant detrital and biogenic magnetites. Minor framboidal iron oxides were also  
266 identified using SEM, optical microscope, and Raman spectrum investigations. However, the  
267 magnetic minerals in these framboids are pigment hematite and/or goethite rather than authigenic  
268 magnetite. Therefore, the ChRMs of the limestones from the Zongpu Formation in the Gamba area  
269 are carried by detrital and biogenic magnetites. The arguments of chemical remagnetization, based on  
270 oversimplified semiquantitative EDS analyses and incomplete rock magnetic measurements in  
271 previous studies, should be rejected. Instead, the paleomagnetic data obtained from the Paleocene  
272 carbonates in the Gamba area can be used for tectonic reconstructions. We suggest that  
273 comprehensive analyses of magnetic extracts with advanced EBSD and TEM are extremely  
274 important and favorable to diagnose the substantial magnetization carriers in carbonate rocks. The  
275 remagnetization hypotheses in Paleocene carbonates from the Tingri area, Tethyan Himalaya, and the  
276 Late Triassic carbonates from the Qiangtang terrane require further study based on the thorough  
277 petrographic and mineralogical investigations to determine the origin of the magnetization.

## 278 **6 Funding**

279 This study was supported by grants from the National Natural Science Foundation of China (Grants  
280 No. 92055205, 41888101) and the Second Tibetan Plateau Scientific Expedition and Research  
281 Program (STEP; Grant No. 2019QZKK0703).

## 282 **7 Acknowledgments**

283 We are grateful to Xu Tang at the Electron Microscopy Laboratory, IGGCAS for helping with TEM  
284 operation and David Richard and Richard T. Wilkin for helpful discussion.

## 285 **1 References**

- 286 Aitchison, J.C., Ali, J.R., and Davis, A.M. (2007). When and where did India and Asia collide?  
287 *Journal of Geophysical Research* 112(B5). doi: 10.1029/2006jb004706.
- 288 Ali, J.R., and Aitchison, J.C. (2008). Gondwana to Asia: Plate tectonics, paleogeography and the  
289 biological connectivity of the Indian sub-continent from the Middle Jurassic through latest  
290 Eocene (166–35Ma). *Earth-Science Reviews* 88, 145-166. doi:  
291 10.1016/j.earscirev.2008.01.007.

- 292 An, W., Hu, X., Garzanti, E., Wang, J.G., and Liu, Q. (2021). New Precise Dating of the India - Asia  
293 Collision in the Tibetan Himalaya at 61 Ma. *Geophysical Research Letters* 48(3). doi:  
294 10.1029/2020gl090641.
- 295 Besse, J., Courtillot, V., Pozzi, J., Westphal, M., and Zhou, Y. (1984). Palaeomagnetic estimates of  
296 crustal shortening in the Himalayan thrusts and Zangbo suture. *Nature* 311(5987), 621-626.  
297 doi: 10.1038/311621a0.
- 298 Brownlow, A.E., Hunter, W., and Parkin, D.W. (1966). Cosmic Spherules in a Pacific Core.  
299 *Geophysical Journal International* 12(1), 1-13. doi: 10.1111/j.1365-246X.1966.tb03096.x.
- 300 Chang, L., Roberts, A.P., Heslop, D., Hayashida, A., Li, J., Zhao, X., et al. (2016). Widespread  
301 occurrence of silicate - hosted magnetic mineral inclusions in marine sediments and their  
302 contribution to paleomagnetic recording. *Journal of Geophysical Research: Solid Earth* 121,  
303 8415-8431. doi: 10.1002/2016JB013109.
- 304 Chang, S., Kirschvink, J.L., and Stolz, J.F. (1987). Biogenic magnetite as a primary remanence  
305 carrier in limestone deposits. *Physics of the Earth and Planetary Interiors* 46(1-3), 289-303.  
306 doi: 10.1016/0031-9201(87)90191-9.
- 307 Channell, J.E.T., and McCabe, C. (1994). Comparison of magnetic hysteresis parameters of  
308 unremagnetized and remagnetized limestones. *Journal of Geophysical Research: Solid Earth*  
309 99(B3), 4613-4623. doi: 10.1029/93JB02578.
- 310 Ding, L., Kapp, P., and Wan, X. (2005). Paleocene - Eocene record of ophiolite obduction and initial  
311 India - Asia collision, south central Tibet. *Tectonics* 24(3). doi: 10.1029/2004TC001729.
- 312 Dunlop, D.J., and Özdemir, Ö. (1997). *Rock magnetism: fundamentals and frontiers*. Cambridge  
313 university press.
- 314 Dupont-Nivet, G., Lippert, P.C., Van Hinsbergen, D.J.J., Meijers, M.J.M., and Kapp, P. (2010).  
315 Palaeolatitude and age of the Indo-Asia collision: palaeomagnetic constraints. *Geophysical*  
316 *Journal International* 182(3), 1189-1198. doi: 10.1111/j.1365-246X.2010.04697.x.
- 317 Elmore, R.D., Lee-Egger Foucher, J., Evans, M., Lewchuk, M., and Cox, E. (2006). Remagnetization  
318 of the Tonoloway Formation and the Helderberg Group in the Central Appalachians: testing  
319 the origin of syntilting magnetizations. *Geophysical Journal International* 166(3), 1062-1076.  
320 doi: 10.1111/j.1365-246X.2006.02875.x.
- 321 Franke, C., Pennock, G., Drury, M.R., Engelmann, R., Lattard, D., Garming, J.F.L., et al. (2007).  
322 Identification of magnetic Fe-Ti oxides in marine sediments by electron backscatter  
323 diffraction in scanning electron microscopy. *Geophysical Journal International* 170(2), 545-  
324 555. doi: 10.1111/j.1365-246X.2007.03410.x.
- 325 Gu, X., Heaney, P.J., Reis, F.D.A., and Brantley, S.L. (2020). Deep abiotic weathering of pyrite.  
326 *Science* 370(6515). doi: 10.1126/science.abb8092.
- 327 Hanesch, M. (2009). Raman spectroscopy of iron oxides and (oxy) hydroxides at low laser power and  
328 possible applications in environmental magnetic studies. *Geophysical Journal International*  
329 177(3), 941-948. doi: 10.1111/j.1365-246X.2009.04122.x.



- 330 Hounslow, M.W., Maher, B.A., Walden, J., Oldfield, F., and Smith, J. (1999). Laboratory procedures  
331 for quantitative extraction and analysis of magnetic minerals from sediments. *Environmental*  
332 *Magnetism, A Practical Guide. Quaternary Research Association, Technical Guide 6*, 139-  
333 164.
- 334 Hu, X., Garzanti, E., Wang, J., Huang, W., An, W., and Webb, A. (2016). The timing of India-Asia  
335 collision onset—Facts, theories, controversies. *Earth-Science Reviews* 160, 264-299. doi:  
336 10.1016/j.earscirev.2016.07.014.
- 337 Huang, W., Jackson, M.J., Dekkers, M.J., Zhang, Y., Zhang, B., Guo, Z., et al. (2019). Challenges in  
338 isolating primary remanent magnetization from Tethyan carbonate rocks on the Tibetan  
339 Plateau: Insight from remagnetized Upper Triassic limestones in the eastern Qiangtang block.  
340 *Earth and Planetary Science Letters* 523, 115695. doi: 10.1016/j.epsl.2019.06.035.
- 341 Huang, W., Lippert, P.C., Jackson, M.J., Dekkers, M.J., Zhang, Y., Li, J., et al. (2017a).  
342 Remagnetization of the Paleogene Tibetan Himalayan carbonate rocks in the Gamba area:  
343 Implications for reconstructing the lower plate in the India-Asia collision. *Journal of*  
344 *Geophysical Research-Solid Earth* 122(2), 808-825. doi: 10.1002/2016jb013662.
- 345 Huang, W., Lippert, P.C., Zhang, Y., Jackson, M.J., Dekkers, M.J., Li, J., et al. (2017b).  
346 Remagnetization of carbonate rocks in southern Tibet: Perspectives from rock magnetic and  
347 petrographic investigations. *Journal of Geophysical Research: Solid Earth* 122(4), 2434-  
348 2456. doi: 10.1002/2017jb013987.
- 349 Jackson, M. (1990). Diagenetic sources of stable remanence in remagnetized Paleozoic cratonic  
350 carbonates: A rock magnetic study. *Journal of Geophysical Research: Solid Earth* 95(B3),  
351 2753-2761. doi: 10.1029/JB095iB03p02753.
- 352 Jackson, M., and Swanson-Hysell, N.L. (2012). Rock magnetism of remagnetized carbonate rocks:  
353 Another look. *Geological Society, London, Special Publications* 371(1), 229-251. doi:  
354 10.1144/SP371.3.
- 355 Jagoutz, O., Macdonald, F.A., and Royden, L. (2016). Low-latitude arc–continent collision as a  
356 driver for global cooling. *Proceedings of the National Academy of Sciences* 113(18), 4935-  
357 4940. doi: 10.1073/pnas.1523667113.
- 358 Kirschvink, J.L., and Lowenstam, H.A. (1979). Mineralization and magnetization of chiton teeth:  
359 paleomagnetic, sedimentologic, and biologic implications of organic magnetite. *Earth and*  
360 *Planetary Science Letters* 44(2), 193-204. doi: 10.1016/0012-821X(79)90168-7.
- 361 Kopp, R.E., and Kirschvink, J.L. (2008). The identification and biogeochemical interpretation of  
362 fossil magnetotactic bacteria. *Earth-Science Reviews* 86(1), 42-61. doi:  
363 10.1016/j.earscirev.2007.08.001.
- 364 Leech, M.L., Singh, S., Jain, A., Klemperer, S.L., and Manickavasagam, R. (2005). The onset of  
365 India–Asia continental collision: early, steep subduction required by the timing of UHP  
366 metamorphism in the western Himalaya. *Earth and Planetary Science Letters* 234(1-2), 83-  
367 97. doi: 10.1016/j.epsl.2005.02.038.

- 368 Li, J., and Hu, X. (2020). A photomicrograph dataset of Late Cretaceous to Early Paleogene  
369 carbonate rocks in Tibetan Himalaya. *China Scientific Data* 5. doi:  
370 10.11922/csdata.2020.0072.zh.
- 371 Li, J., Hu, X., Garzanti, E., An, W., and Wang, J. (2015). Paleogene carbonate microfacies and  
372 sandstone provenance (Gamba area, South Tibet): Stratigraphic response to initial India–Asia  
373 continental collision. *Journal of Asian Earth Sciences* 104, 39-54. doi:  
374 10.1016/j.jseas.2014.10.027.
- 375 Ma, Y., Yang, T., Bian, W., Jin, J., Zhang, S., Wu, H., et al. (2016). Early Cretaceous paleomagnetic  
376 and geochronologic results from the Tethyan Himalaya: Insights into the Neotethyan  
377 paleogeography and the India-Asia collision. *Sci Rep* 6, 21605. doi: 10.1038/srep21605.
- 378 McCabe, C., and Elmore, R.D.J.R.o.G. (1989). The occurrence and origin of late Paleozoic  
379 remagnetization in the sedimentary rocks of North America. 27(4), 471-494.
- 380 Meert, J.G., Pivarunas, A.F., Evans, D., Pisarevsky, S.A., and Salminen, J.M. (2020). The  
381 magnificent seven: A proposal for modest revision of the quality index. *Tectonophysics*  
382 790(5), 228549. doi: 10.1016/j.tecto.2020.228549.
- 383 Meng, J., Gilder, S.A., Wang, C., Coe, R.S., Tan, X., Zhao, X., et al. (2019). Defining the Limits of  
384 Greater India. *Geophysical Research Letters*. doi: 10.1029/2019gl082119.
- 385 Meng, J., Lhuillier, F., Wang, C., Liu, H., Eid, B., and Li, Y. (2020). Paleomagnetism of Paleocene -  
386 Maastrichtian (60 - 70 Ma) Lava Flows From Tian Shan (Central Asia): Directional Analysis  
387 and Paleointensities. *Journal of Geophysical Research: Solid Earth* 125(9), e2019JB018631.  
388 doi: 10.1029/2019JB018631.
- 389 Najman, Y., Appel, E., Boudagher-Fadel, M., Bown, P., Carter, A., Garzanti, E., et al. (2010).  
390 Timing of India-Asia collision: Geological, biostratigraphic, and palaeomagnetic constraints.  
391 *Journal of Geophysical Research* 115(B12). doi: 10.1029/2010jb007673.
- 392 Newell, A.J., and Merrill, R.T. (2000). Size dependence of hysteresis properties of small pseudo -  
393 single - domain grains. *Journal of Geophysical Research: Solid Earth* 105(B8), 19393-  
394 19403. doi: 10.1029/2000JB900122.
- 395 Patriat, P., and Achache, J. (1984). India-Eurasia collision chronology has implications for crust  
396 shortening and diving mechanism of plates. *Nature* 311(18), 615-621. doi: 10.1038/311615a0
- 397 Patzelt, A., Li, H., Wang, J., and Appel, E. (1996). Palaeomagnetism of Cretaceous to Tertiary  
398 sediments from southern Tibet: evidence for the extent of the northern margin of India prior  
399 to the collision with Eurasia. *Tectonophysics* 259(4), 259-284. doi: 10.1016/0040-  
400 1951(95)00181-6.
- 401 Roberts, A.P. (2015). Magnetic mineral diagenesis. *Earth-Science Reviews* 151, 1-47. doi:  
402 10.1016/j.earscirev.2015.09.010
- 403 Roberts, A.P., Chang, L., Rowan, C.J., Horng, C.S., and Florindo, F. (2011). Magnetic properties of  
404 sedimentary greigite (Fe<sub>3</sub>S<sub>4</sub>): An update. *Reviews of Geophysics* 49(1). doi: 10.1016/0012-  
405 821X(95)00131-U.

- 406 Roberts, A.P., Cui, Y., and Verosub, K.L. (1995). Wasp - waisted hysteresis loops: Mineral magnetic  
407 characteristics and discrimination of components in mixed magnetic systems. *Journal of*  
408 *Geophysical Research: Solid Earth* 100(B9), 17909-17924. doi: 10.1029/95JB00672.
- 409 Roberts, A.P., Tauxe, L., Heslop, D., Zhao, X., and Jiang, Z. (2018). A Critical Appraisal of the  
410 “Day” Diagram. *Journal of Geophysical Research: Solid Earth* 123(4), 2618-2644. doi:  
411 10.1002/2017JB015247.
- 412 Saffer, B., and McCabe, C. (1992). Further studies of carbonate remagnetization in the northern  
413 Appalachian basin. *Journal of Geophysical Research: Solid Earth* 97(B4), 4331-4348. doi:  
414 10.1029/91JB02746.
- 415 Sgavetti, M., Pompilio, L., Roveri, M., Manzi, V., Valentino, G., Lugli, S., et al. (2009). Two  
416 geologic systems providing terrestrial analogues for the exploration of sulfate deposits on  
417 Mars: Initial spectral characterization. *Planetary and Space Science* 57(5-6), 614-627. doi:  
418 10.1016/j.pss.2008.05.010.
- 419 Suk, D., and Halgedahl, S.L. (1996). Hysteresis properties of magnetic spherules and whole rock  
420 specimens from some Paleozoic platform carbonate rocks. *Journal of Geophysical Research:*  
421 *Solid Earth* 101(B11), 25053-25075. doi: 10.1029/96JB02271.
- 422 Suk, D., Peacor, D., and Van der Voo, R. (1990). Replacement of pyrite framboids by magnetite in  
423 limestone and implications for palaeomagnetism. *Nature* 345(6276), 611-613. doi:  
424 10.1038/345611a0.
- 425 Suk, D., Van der Voo, R., and Peacor, D.R. (1992). SEM/STEM observation of magnetic minerals in  
426 presumably unremagnetized Paleozoic carbonates from Indiana and Alabama. *Tectonophysics*  
427 215(3-4), 255-272. doi: 10.1016/0040-1951(92)90356-B.
- 428 Sun, W., and Jackson, M. (1994). Scanning electron microscopy and rock magnetic studies of  
429 magnetic carriers in remagnetized early Paleozoic carbonates from Missouri. *Journal of*  
430 *Geophysical Research: Solid Earth* 99(B2), 2935-2942. doi: 10.1029/93JB02761.
- 431 Tarduno, J.A., Cottrell, R.D., and Smirnov, A.V. (2006). The paleomagnetism of single silicate  
432 crystals: Recording geomagnetic field strength during mixed polarity intervals, superchrons,  
433 and inner core growth. *Reviews of Geophysics* 44(1), RG1002. doi: 10.1029/2005RG000189.
- 434 Tarduno, J.A., Cottrell, R.D., Watkeys, M.K., Hofmann, A., Doubrovine, P.V., Mamajek, E.E., et al.  
435 (2010). Geodynamo, Solar Wind, and Magnetopause 3.4 to 3.45 Billion Years Ago. *Science*  
436 327(5970), 1238-1240. doi: 10.1126/science.1183445.
- 437 Tauxe, L., Mullender, T., and Pick, T. (1996). Potbellies, wasp - waists, and superparamagnetism in  
438 magnetic hysteresis. *Journal of Geophysical Research: Solid Earth* 101(B1), 571-583.
- 439 Todd, E.C., Sherman, D.M., and Purton, J.A. (2003). Surface oxidation of pyrite under ambient  
440 atmospheric and aqueous (pH= 2 to 10) conditions: electronic structure and mineralogy from  
441 X-ray absorption spectroscopy. *Geochimica et Cosmochimica Acta* 67(5), 881-893. doi:  
442 10.1016/S0016-7037(02)00957-2.

- 443 Tong, Y., Yang, Z., Zheng, L., Yang, T., Shi, L., Sun, Z., et al. (2008). Early Paleocene  
444 paleomagnetic results from southern Tibet, and tectonic implications. *International Geology*  
445 *Review* 50(6), 546-562. doi: 10.2747/0020-6814.50.6.546
- 446 van Hinsbergen, D.J.J., Lippert, P.C., Dupont-Nivet, G., McQuarrie, N., Doubrovine, P.V., Spakman,  
447 W., et al. (2012). Greater India Basin hypothesis and a two-stage Cenozoic collision between  
448 India and Asia. *Proceedings of the National Academy of Sciences* 109(20), 7659-7664. doi:  
449 10.1073/pnas.1117262109.
- 450 van Hinsbergen, D.J.J., Steinberger, B., Doubrovine, P.V., and Gassmöller, R. (2011). Acceleration  
451 and deceleration of India-Asia convergence since the Cretaceous: Roles of mantle plumes and  
452 continental collision. *Journal of Geophysical Research* 116(B6). doi: 10.1029/2010jb008051.
- 453 Verron, H., Sterpenich, J., Bonnet, J., Bourdelle, F., Mosser-Ruck, R., Lorgeoux, C., et al. (2019).  
454 Experimental study of pyrite oxidation at 100° C: implications for deep geological radwaste  
455 repository in claystone. *Minerals* 9(7), 427. doi: 10.3390/min9070427.
- 456 Wan, X., Jansa, L.F., and Sarti, M. (2002a). Cretaceous and Paleogene boundary strata in southern  
457 Tibet and their implication for the India - Eurasia collision. *Lethaia* 35(2), 131-146. doi:  
458 10.1080/002411602320183999.
- 459 Wan, X., Liang, D., and Li, G. (2002b). Palaeocene strata in Gamba, Tibet and influence of  
460 tectonism. *Acta Geologica Sinica* 76(2), 155-162. doi: 10.3321/j.issn:0001-5717.2002.02.002
- 461 Wang, X., Wan, X., and Li, G. (2008). Late Cretaceous to early Paleogene strontium isotopic  
462 stratigraphy in the Gamba area, Tibet. *Geology in China* 4, 598-607. doi: 10.3969/j.issn.1000-  
463 3657.2008.04.004
- 464 Weil, A.B., and Van der Voo, R. (2002). Insights into the mechanism for orogen - related carbonate  
465 remagnetization from growth of authigenic Fe - oxide: A scanning electron microscopy and  
466 rock magnetic study of Devonian carbonates from northern Spain. *Journal of Geophysical*  
467 *Research: Solid Earth* 107(B4), EPM 1-1-EPM 1-14. doi: 10.1029/2001JB000200.
- 468 Willems, H., and Zhang, B. (1993). Cretaceous and lower Tertiary sediments of the Tibetan Tethys  
469 Himalaya in the area of Tingri (South Tibet, PR China). *Geoscientific Investigation in the*  
470 *Tethyan Himalayas. Berichte aus dem Fachbereich Geowissenschaften der Universität*  
471 *Bremen* 38, 28-47.
- 472 Xu, W., Van der Voo, R., and Peacor, D.R. (1994). Are magnetite spherules capable of carrying  
473 stable magnetizations? *Geophysical Research letters* 21(7), 517-520. doi:  
474 10.1029/94GL00366.
- 475 Xu, W., Van der Voo, R., and Peacor, D.R. (1998). Electron microscopic and rock magnetic study of  
476 remagnetized Leadville carbonates, central Colorado. *Tectonophysics* 296(3-4), 333-362. doi:  
477 10.1016/S0040-1951(98)00146-2.
- 478 Yang, T., Jin, J., Bian, W., Ma, Y., Gao, F., Peng, W., et al. (2019). Precollisional Latitude of the  
479 Northern Tethyan Himalaya From the Paleocene Redbeds and Its Implication for Greater  
480 India and the India-Asia collision. *Journal of Geophysical Research: Solid Earth* 124(11),  
481 10777-10798. doi: 10.1029/2019JB017927.

- 482 Yang, T., Ma, Y., Bian, W., Jin, J., Zhang, S., Wu, H., et al. (2015). Paleomagnetic results from the  
 483 Early Cretaceous Lakang Formation lavas: Constraints on the paleolatitude of the Tethyan  
 484 Himalaya and the India–Asia collision. *Earth and Planetary Science Letters* 428, 120-133.  
 485 doi: 10.1016/j.epsl.2015.07.040.
- 486 Yi, Z., Appel, E., and Huang, B. (2017). Comment on "Remagnetization of the Paleogene Tibetan  
 487 Himalayan carbonate rocks in the Gamba area: Implications for reconstructing the lower plate  
 488 in the India-Asia collision" by Huang et al. *Journal of Geophysical Research-Solid Earth*  
 489 122(7), 4852-4858. doi: 10.1002/2017jb014353.
- 490 Yi, Z., Huang, B., Chen, J., Chen, L., and Wang, H. (2011). Paleomagnetism of early Paleogene  
 491 marine sediments in southern Tibet, China: Implications to onset of the India-Asia collision  
 492 and size of Greater India. *Earth and Planetary Science Letters* 309(1-2), 153-165. doi:  
 493 10.1016/j.epsl.2011.07.001.
- 494 Yi, Z., Wang, T., Meert, J.G., Zhao, Q., and Liu, Y. (2021). An Initial Collision of India and Asia in  
 495 the Equatorial Humid Belt. *Geophysical Research Letters* 48(9), e2021GL093408. doi:  
 496 10.1029/2021GL093408.
- 497 Yin, A., and Harrison, T.M. (2000). Geologic evolution of the Himalayan-Tibetan orogen. *Annual*  
 498 *Review of Earth and Planetary Sciences* 28(1), 211-280. doi: 10.1146/annurev.earth.28.1.211.
- 499 Yuan, J., Yang, Z., Deng, C., Krijgsman, W., Hu, X., Li, S., et al. (2020). Rapid drift of the Tethyan  
 500 Himalaya terrane before two-stage India-Asia collision. *National Science Review*. doi:  
 501 10.1093/nsr/nwaa173.
- 502 Zhang, Q., Willems, H., Ding, L., and Xu, X. (2019a). Response of larger benthic foraminifera to the  
 503 Paleocene-Eocene thermal maximum and the position of the Paleocene/Eocene boundary in  
 504 the Tethyan shallow benthic zones: Evidence from south Tibet. *Geological Society of*  
 505 *America Bulletin* 131(1-2), 84-98. doi: 10.1130/B31813.1.
- 506 Zhang, Y., Huang, B.C., and Zhao, Q. (2019b). New paleomagnetic positive proof of the rigid or  
 507 quasi-rigid Greater Indian Plate during the Early Cretaceous. *Chinese Science Bulletin* 64(21),  
 508 2225-2244. doi: 10.1360/n972019-00196.
- 509 Zwing, A., Matzka, J., Bachtadse, V., and Soffel, H. (2005). Rock magnetic properties of  
 510 remagnetized Palaeozoic clastic and carbonate rocks from the NE Rhenish massif, Germany.  
 511 *Geophysical Journal International* 160(2), 477-486. doi: 10.1111/j.1365-246X.2004.02493.x.

## 512 2 Figure captions

513 **Figure 1.** (A) Schematic structural map of the India-Asia collision zone. (B) Geologic map of the Gamba area  
 514 with the sampling locations of Yi et al. (2011) (red star) and Huang et al., (2017a) (green star). (C)  
 515 Lithostratigraphy of section A of Yi et al. (2011). Red and blue dots indicate the sampling levels for samples  
 516 collected for thin sections observation and magnetic extraction, respectively.

517 **Figure 2.** Photomicrographs illustrating the iron oxide mineralogical features of limestones from the Zongpu  
 518 Formation in the Gamba area under reflected light (A-D, I-L) and plane-polarized light (E-H, M-P) images.  
 519 Cal = calcite; Gt = goethite; pHem = pigment hematite; Py = pyrite.

520 **Figure 3.** Raman spectrum of the limestones from the Zongpu Formation. Three types of Fe-O-S minerals,  
521 i.e., hematite ( $222\text{ cm}^{-1}$ ,  $297\text{ cm}^{-1}$ , and  $390\text{ cm}^{-1}$ ) (A), goethite ( $208\text{ cm}^{-1}$ ,  $270\text{ cm}^{-1}$  and  $380\text{ cm}^{-1}$ ) (B) and pyrite  
522 ( $344\text{ cm}^{-1}$  and  $379\text{ cm}^{-1}$ ) (C) can be identified in the Raman spectra.

523 **Figure 4.** (A-L) Secondary-electron SEM images of magnetic extracts in limestones of the Zongpu Formation.  
524 (M and P) EBSPs solution of iron oxides corresponding to the white circles indicated in Figure 4 A-C. Zone  
525 axes are labeled using Miller indices. Note the white circle areas are not as accurate as that was shown in the  
526 images, because of the low resolution of SEM during EBSD analyses. White arrows in Figures 4K and 4L  
527 indicate the possible occurrence of biogenic magnetite. White dots represent the EDS spots as shown in Figure  
528 S3. [Fe-O] = iron oxides.

529 **Figure 5.** Elemental mapping exhibits elemental compositions and distributions of an iron-oxidized framboid.  
530 (A) SEM image of a framboid with line scan by energy spectrum. (B-D) Fe, S, and O elements are scattered in  
531 most areas. White arrows show significant variation in the distributions of Fe, O, and S elements.

532 **Figure 6.** High-resolution TEM and SAED analyses of magnetic minerals for magnetic extracts from  
533 limestone in the Zongpu Formation. (A-D) Bright-field TEM images at progressively higher magnifications  
534 reveal characteristics of mixed magnetic particles with different sizes. (E-F) Clear lattice fringes for the  
535 magnetic minerals are observed. (G-I) Ring-like and spot-like SAED patterns and (J-L) EDS spectra of the  
536 magnetic particles in B-D. The particles in different sizes are magnetite (B, C) and titanomagnetite (D).

537

538

539

540

541

Figure 1.JPEG

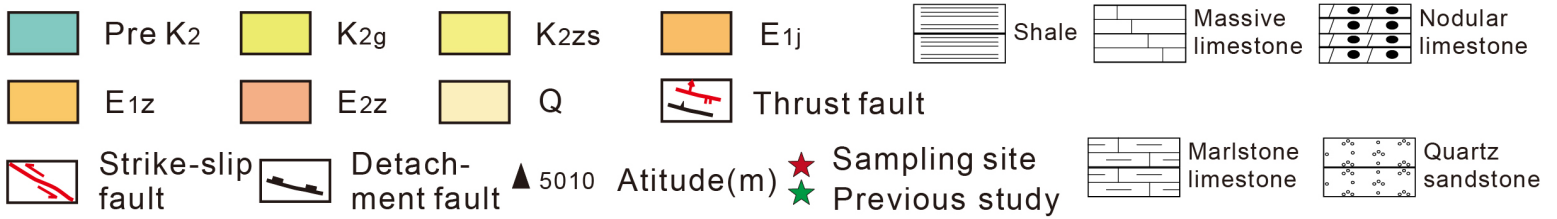
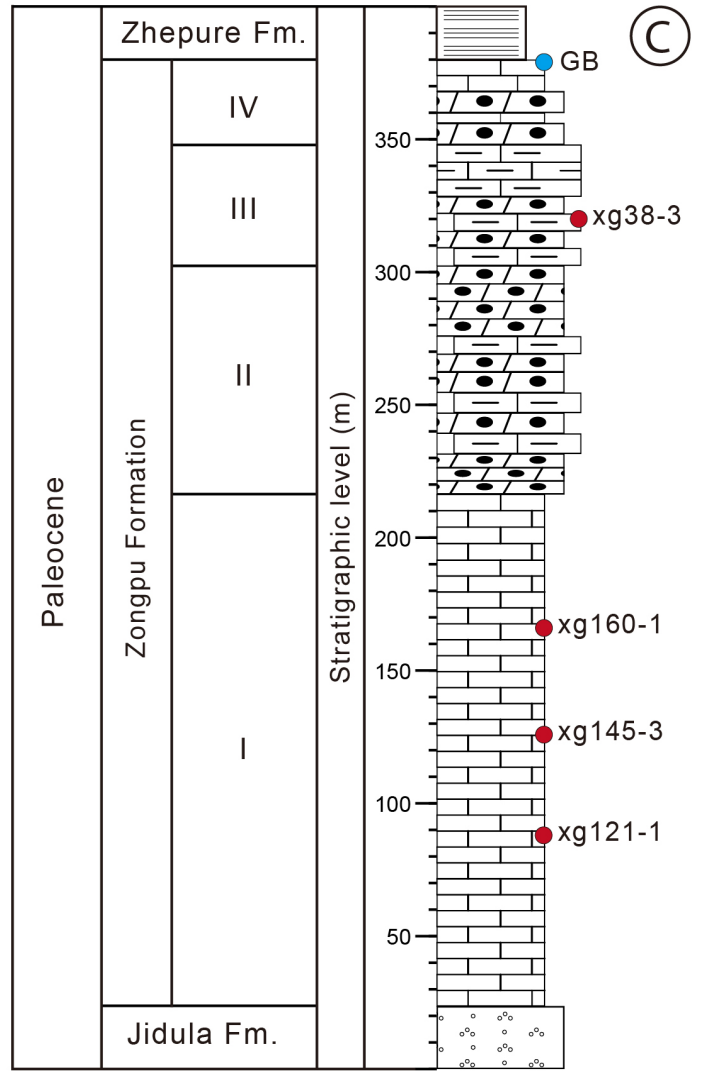
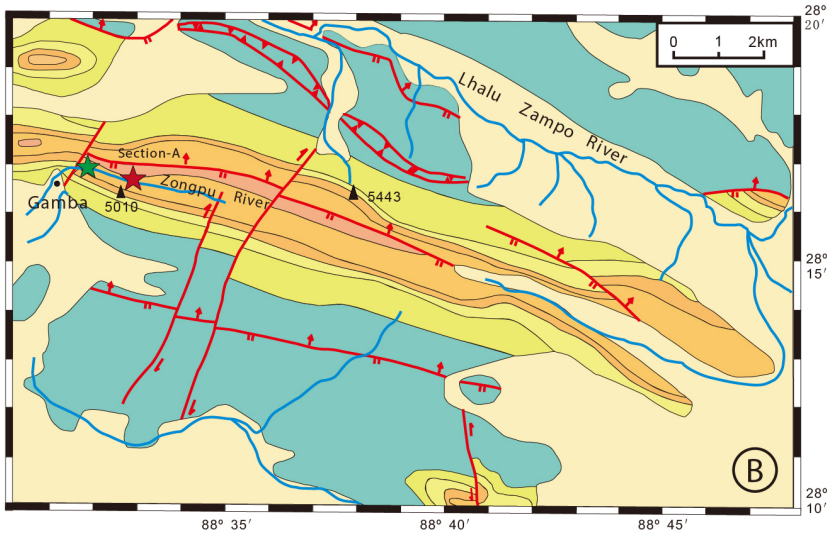
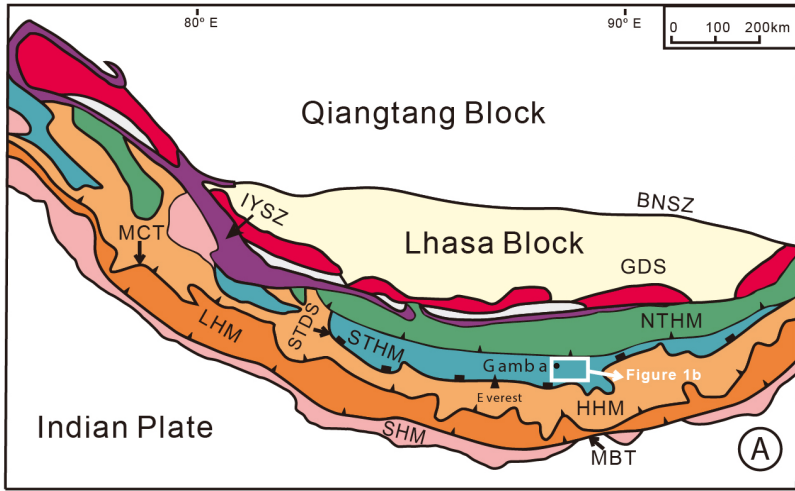


Figure 2.JPEG

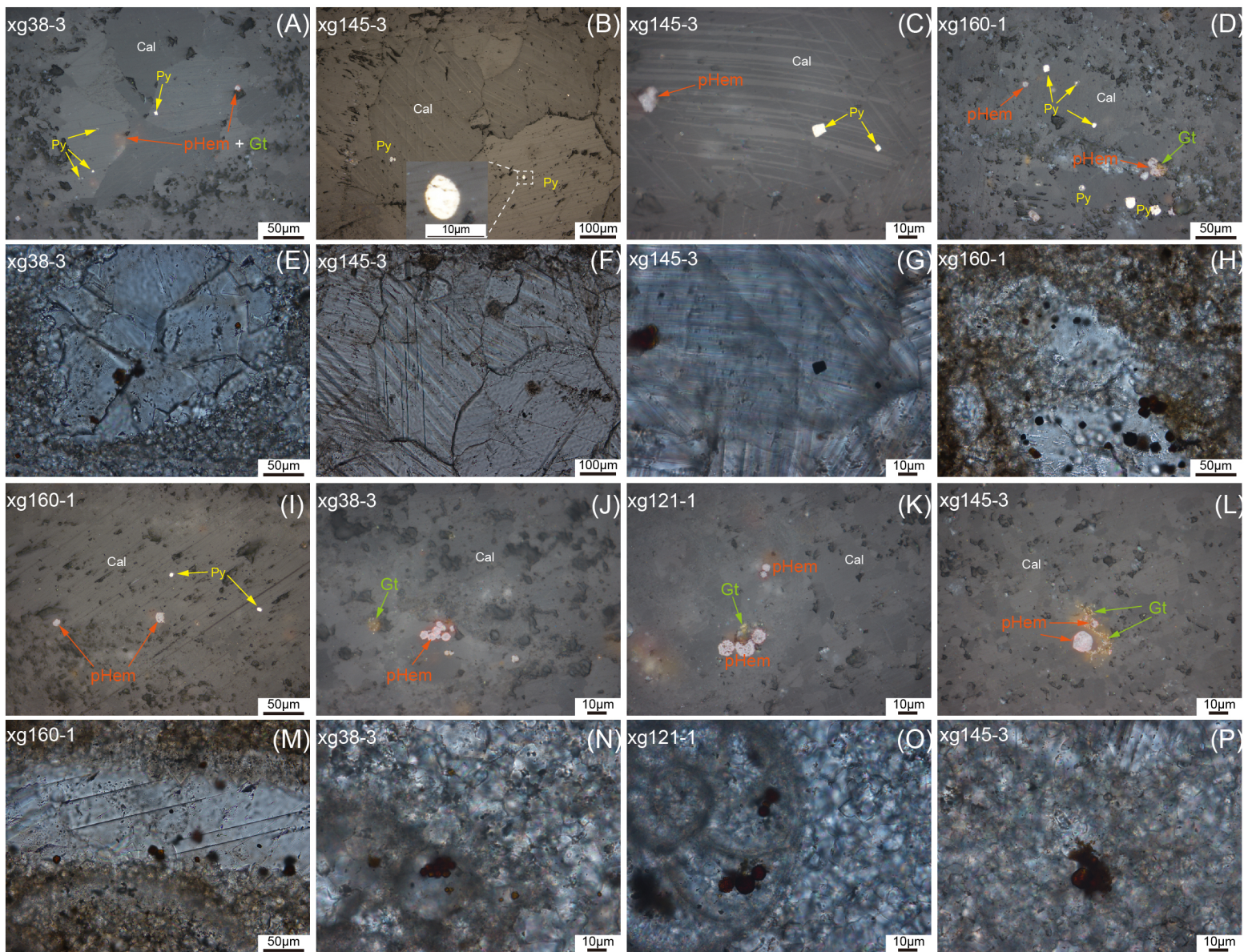




Figure 3.JPEG

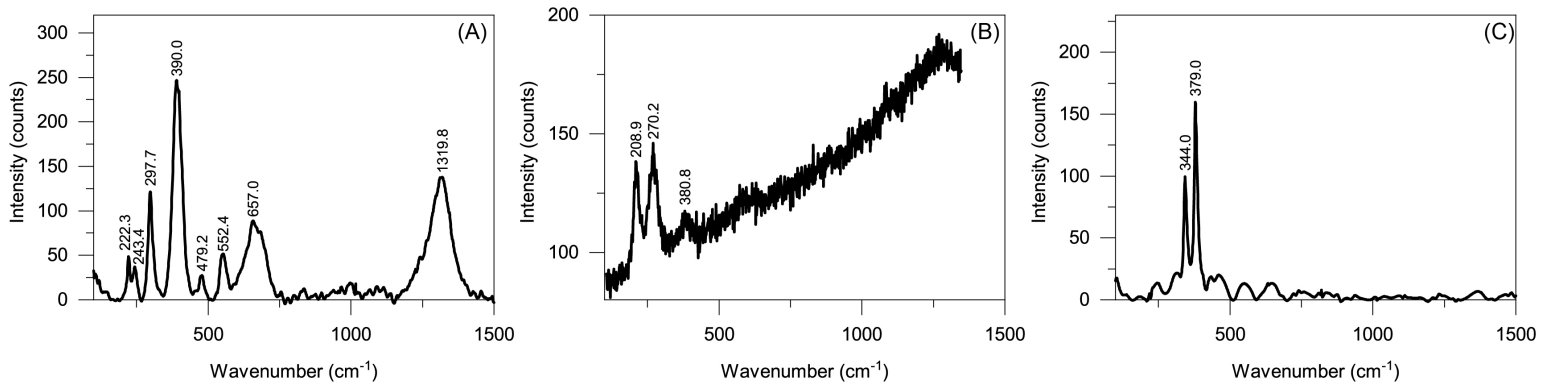


Figure 4.JPEG

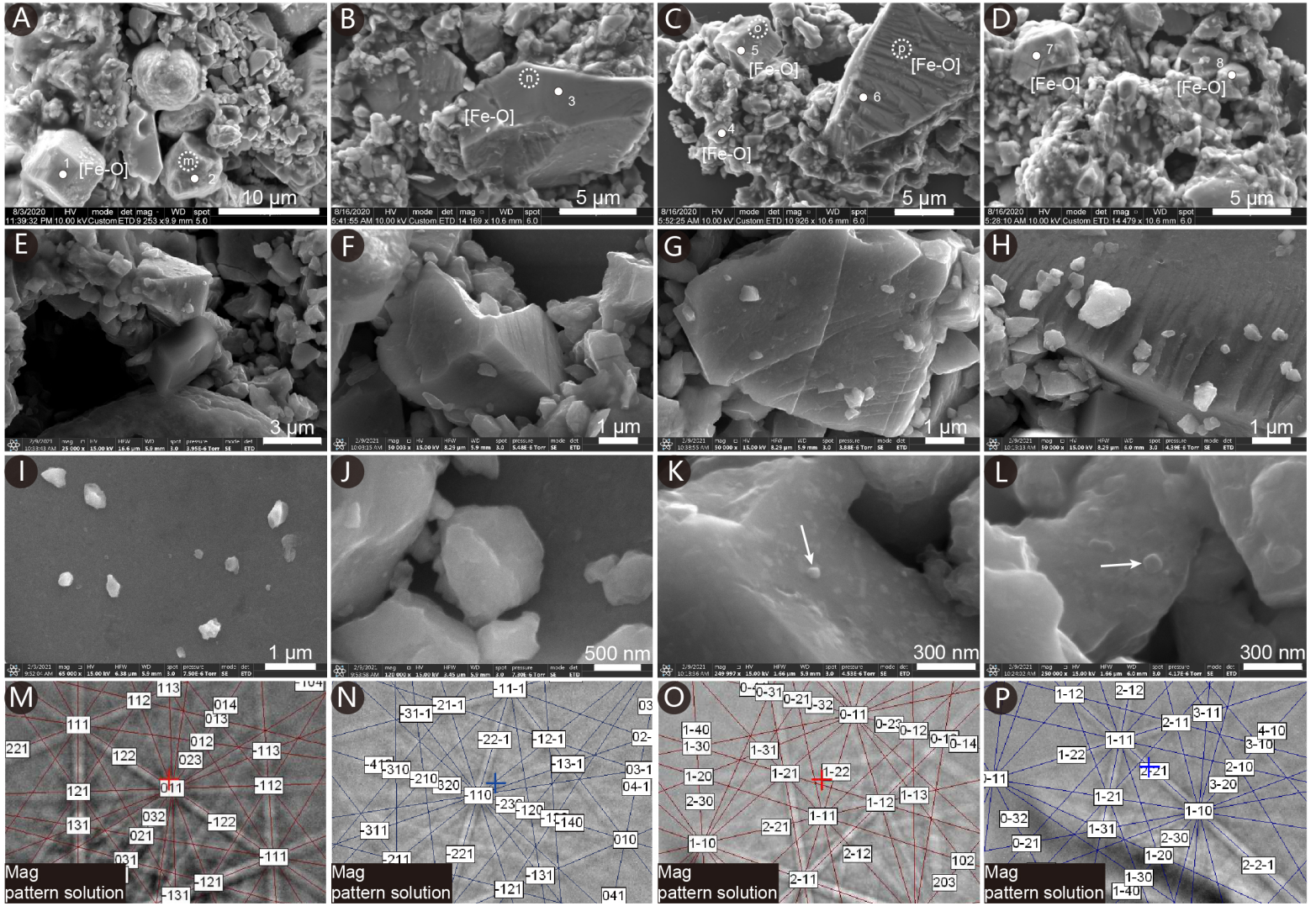


Figure 5.JPEG

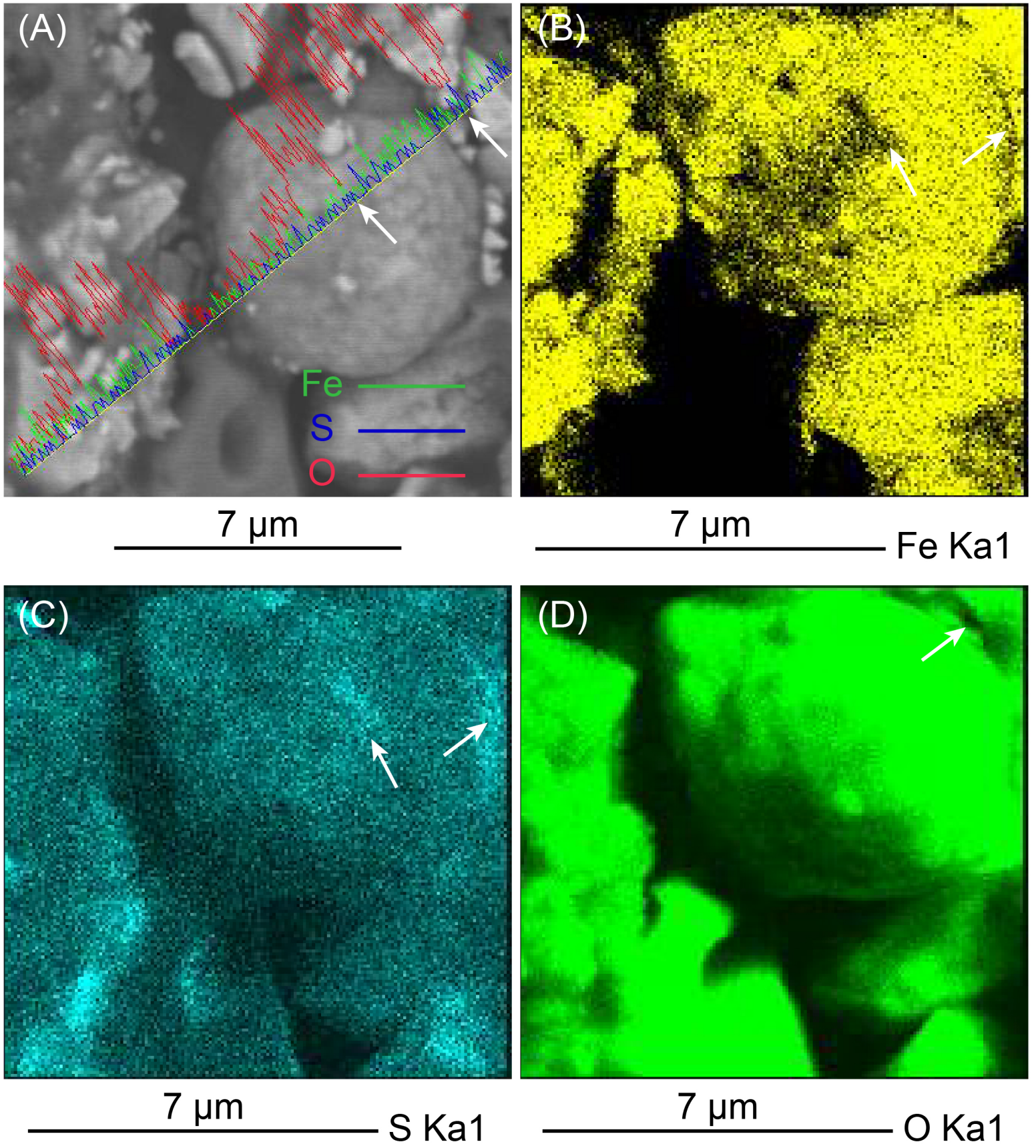
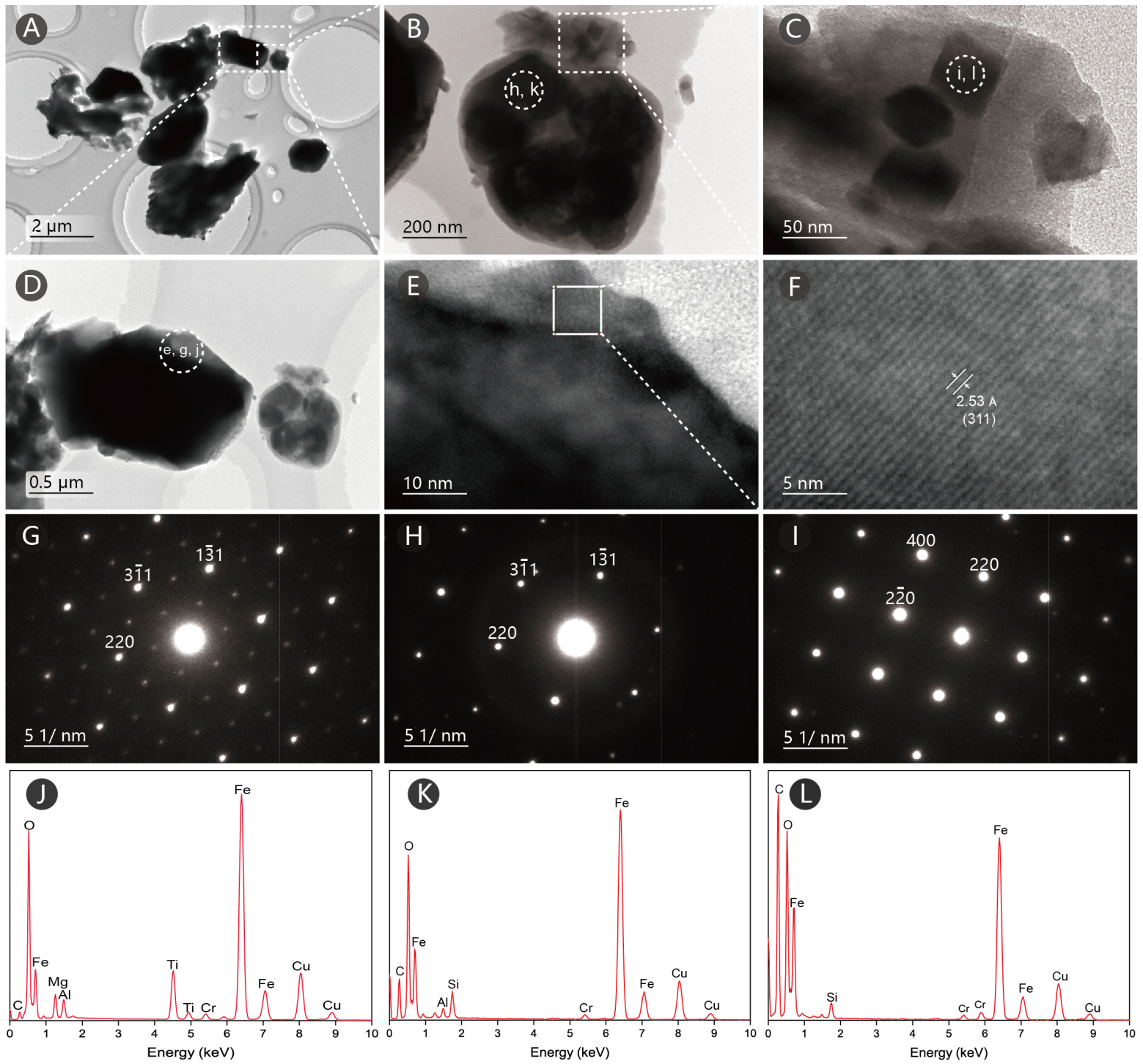
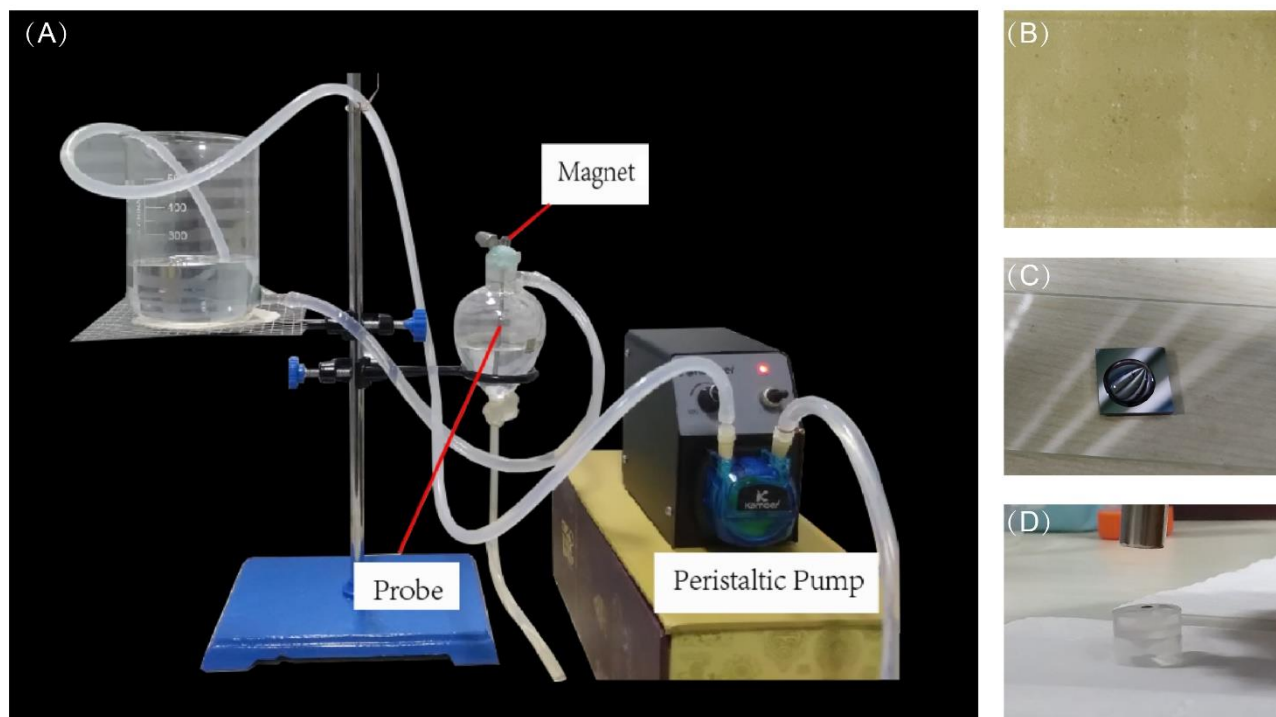


Figure 6.JPEG



## Supplementary Material

### 1 Supplementary Figures



**Figure S1.** (a) Magnetic extraction apparatus. (b) Samples preparation of thin sections using resin as an adhesive; Magnetic extracts dropping on a monocrystalline silicon wafer (c), and TEM grid (d).

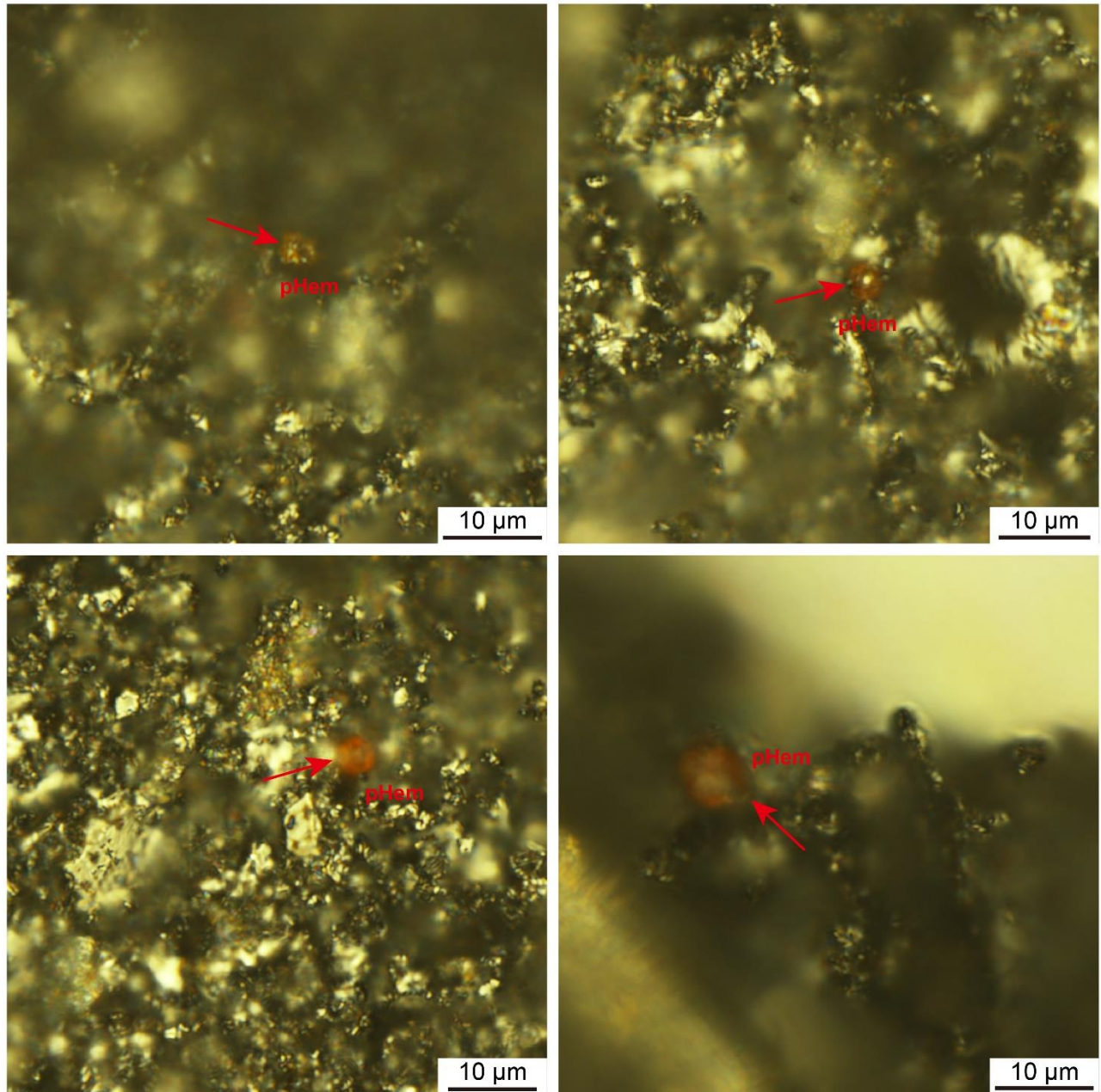


**Figure S2.** Photomicrographs illustrating the iron oxide spherules of magnetic extracts from the Zongpu carbonate rocks in the Gamba area under reflected light. pHem = pigment hematite.

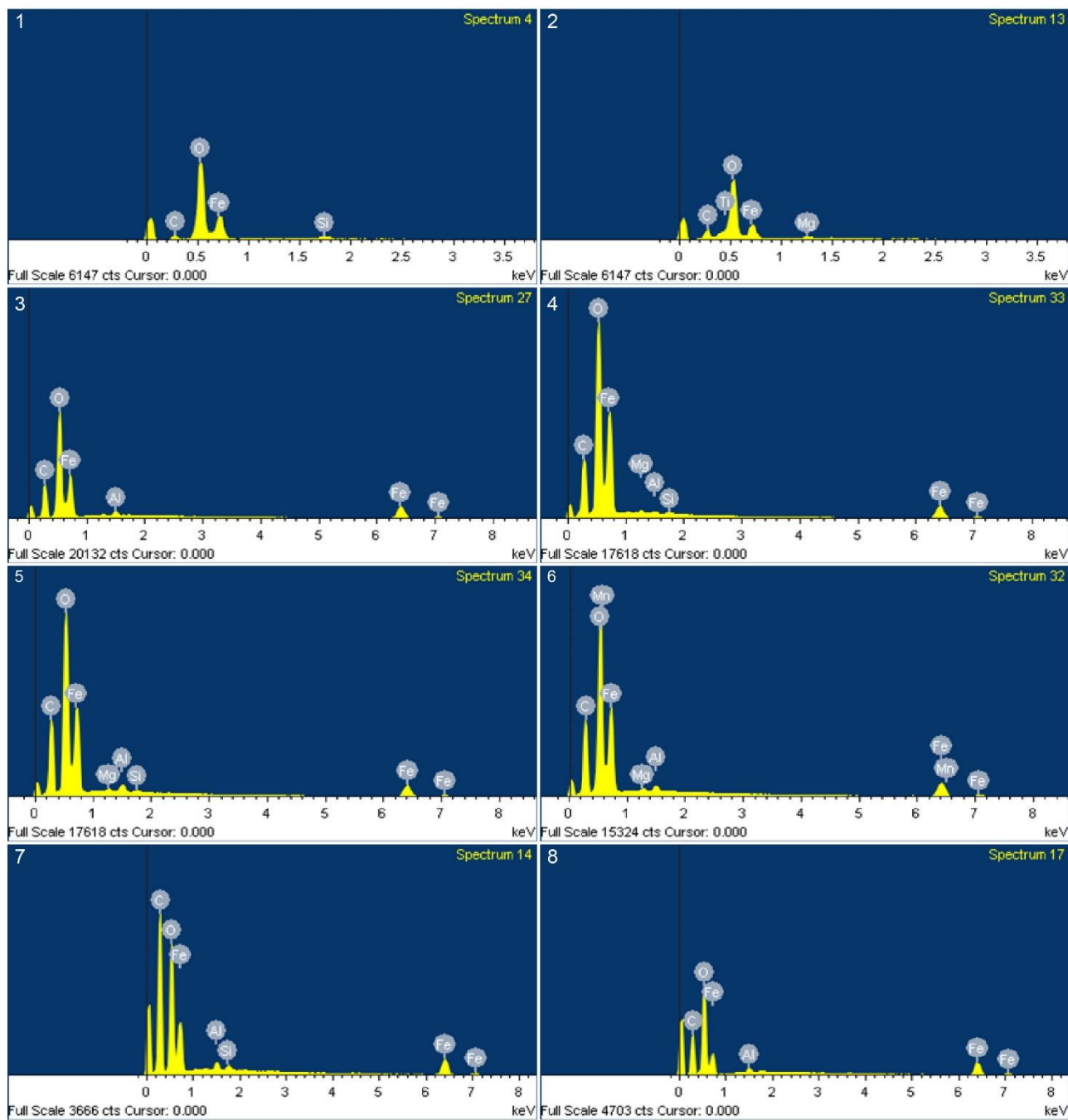


**Figure S3.** EDS analysis results of the spots shown in Figure 4.

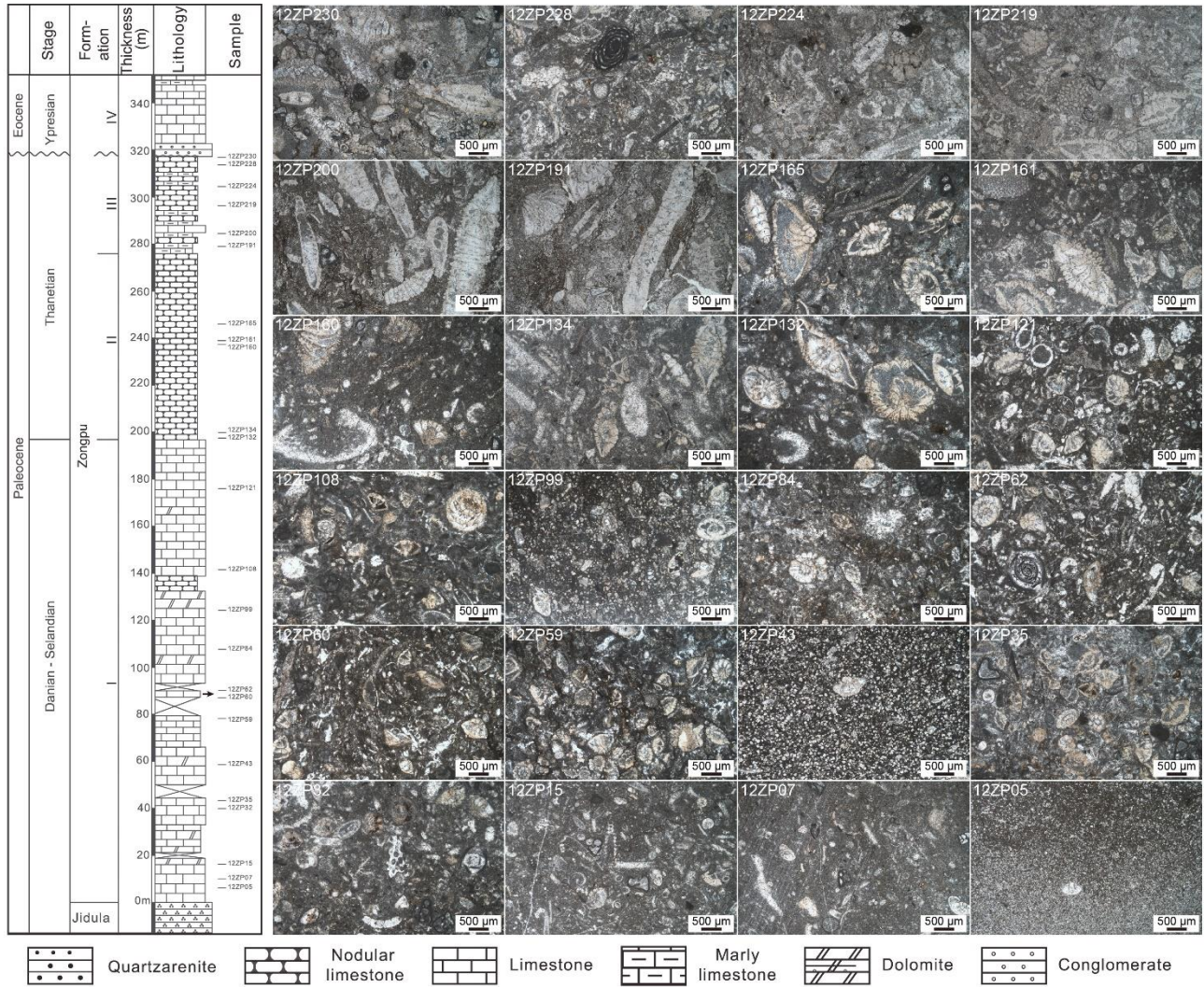


**Figure S4.** Left: Lithostratigraphy of the Zongpu Formation. Partial sampling localities of rock magnetic measurements in Huang et al. (2017a) were indicated, modified after Li et al. (2015) and Huang et al. (2017a). Right: Corresponding photomicrographs, collected from Li and Hu (2020). Please see [www.csdata.org](http://www.csdata.org) for more micrographs and detailed descriptions.



## 2 Reference

- Huang, W., Lippert, P.C., Jackson, M.J., Dekkers, M.J., Zhang, Y., Li, J., et al. (2017a). Remagnetization of the Paleogene Tibetan Himalayan carbonate rocks in the Gamba area: Implications for reconstructing the lower plate in the India-Asia collision. *Journal of Geophysical Research-Solid Earth* 122(2), 808-825. doi: 10.1002/2016jb013662.
- Li, J., Hu, X., Garzanti, E., An, W., and Wang, J. (2015). Paleogene carbonate microfacies and sandstone provenance (Gamba area, South Tibet): Stratigraphic response to initial India–Asia continental collision. *Journal of Asian Earth Sciences* 104, 39-54. doi: 10.1016/j.jseaes.2014.10.027.
- Li, J., and Hu, X. (2020). A photomicrograph dataset of Late Cretaceous to Early Paleogene carbonate rocks in Tibetan Himalaya. *China Scientific Data* 5. doi: 10.11922/csdata.2020.0072.zh.